RF Linearity Characteristics of SiGe HBTs

Guofu Niu, *Member, IEEE*, Qingqing Liang, John D. Cressler, *Fellow, IEEE*, Charles S. Webster, *Member, IEEE*, and David L. Harame, *Member, IEEE*

***Abstract*—Two-tone intermodulation in ultrahigh vacuum/chemical vapor deposition SiGe heterojunction bipolar transistors (HBTs) were analyzed using a Volterra-series-based approach that completely distinguishes individual nonlinearities. Avalanche multiplication and collector–base (CB) capacitance were shown to be the dominant nonlinearities in a single-stage common-emitter amplifier. At a given I_C, an optimum V_{CE} exists for a maximum third-order intercept point (IIP3). The IIP3 is limited by the avalanche multiplication nonlinearity at low I_C, and limited by the C_{CB} nonlinearity at high I_C. The decrease of the avalanche multiplication rate at high I_C is beneficial to linearity in SiGe HBTs. The IIP3 is sensitive to the biasing condition because of strong dependence of the avalanche multiplication current and CB capacitance on I_C and V_{CE}. The load dependence of linearity was attributed to the feedback through the CB capacitance and the avalanche multiplication in the CB junction. Implications on the optimization of the transistor biasing condition and transistor structure for improved linearity are also discussed.**

***Index Terms*—Avalanche multiplication, linearity, nonlinearity cancellation, RF technology, SiGe HBT, Volterra series.**

I. Introduction

RF CIRCUIT applications often require transistors with low intermodulation distortion. Measurement of transistor intermodulation characteristics in the gigahertz range requires substantial experimental effort, and optimization of linearity through device fabrication-measurement iteration can be very time consuming and costly. Thus, linearity analysis and simulation are desired to understand linearity limiting factors for a given technology, as well as to optimize transistor structure and circuit topology for improved linearity. The classical approach to simulating intermodulation distortion is to perform a time-domain transient analysis with two-tone excitation, and then perform Fourier analysis of the output. This approach requires a tremendous amount of simulation time for RF circuits because the RF frequency is several orders of magnitude higher than the baseband frequencies, which results in an enormous number of time steps. Accurate Fourier analysis of signals with closely spaced frequencies is also very difficult. "Shooting methods" and "harmonic balance" methods overcome these problems, and are suitable for general-purpose large-signal distortion analysis [1]. In situations of weak nonlinearity such as small-signal distortion, the Volterra-series approach [2]–[8] can be used. As recently proposed in [4] and further developed in this paper, the dominant nonlinearities can be identified using the Volterra-series method, which is very difficult using other methods. In today's digital mobile communication circuits, many RF amplifiers operate in a region of weak nonlinearity, such as low-noise amplifiers (LNAs) at the RF front end. Therefore, Volterra series is the best approach for identifying the linearity limiting factors of a given transistor technology for these weakly nonlinear applications.

In this paper, we present a systematic analysis of intermodulation in SiGe heterojunction bipolar transistors (HBTs) using the Volterra-series approach. Details of the ultrahigh vacuum/chemical vapor deposition (UHV/CVD) SiGe HBT technology used in this study can be found in [9]. A new method of distinguishing the contributions from individual nonlinearities is proposed. Nonlinearity cancellation and its dependence on transistor parameters, bias, load condition, and feedback are examined using the proposed method. In particular, we examine the impact of avalanche multiplication, which has been a concern for SiGe HBTs because of their inherently low breakdown voltage compared to III–V HBTs. The results show that the negative impact of avalanche multiplication on linearity can be substantially alleviated by proper choice of device bias and circuit topology. The impact of collector profile design, and its implications to RF integrated-circuit (IC) design are also discussed.

II. Transistor Modeling

Distortion analysis demands accurate modeling of transistor I–V and C–V characteristics. Fig. 1 depicts the equivalent circuit used in this study and includes the dominant nonlinearities. I_{CE} represents the collector current transported from the emitter, I_{BE} represents the hole injection into the emitter, and I_{CB} represents the avalanche multiplication current

$$I_{CB} = I_{CE}(M-1) = I_{C0}(V_{BE})F_{\text{Early}}(M-1) \quad (1)$$

where $I_{C0}(V_{BE})$ is the I_C measured at zero V_{CB}, M is the avalanche multiplication factor, and F_{Early} is the Early effect factor [10]. The avalanche multiplication factor M and the Early effect factor F_{Early} were measured using a technique recently proposed [10]. It is important to distinguish the Early effect and avalanche multiplication, though they both contribute to an increase of I_C with increasing V_{CB}, because of their different impacts on the base and emitter currents [10]. The collector–base (CB) capacitance was partitioned by the base resistance through a factor of *XCJC*, as in SPICE. The values of

Manuscript received March 30, 2001. This work was supported by IBM under an IBM University Partner Award and by the Semiconductor Research Corporation under Contract 2000-HJ-769.

G. Niu, Q. Liang, and J. D. Cressler, are with the Alabama Microelectronics Science and Technology Center, Electrical and Computer Engineering Department, Auburn University, Auburn, AL 36849 USA (e-mail: guofu@eng.auburn.edu).

C. S. Webster and D. L. Harame are with IBM Microelectronics, Essex Junction, VT 05452 USA.

Publisher Item Identifier S 0018-9480(01)07580-9.

0018–9480/01$10.00 ©2001 IEEE

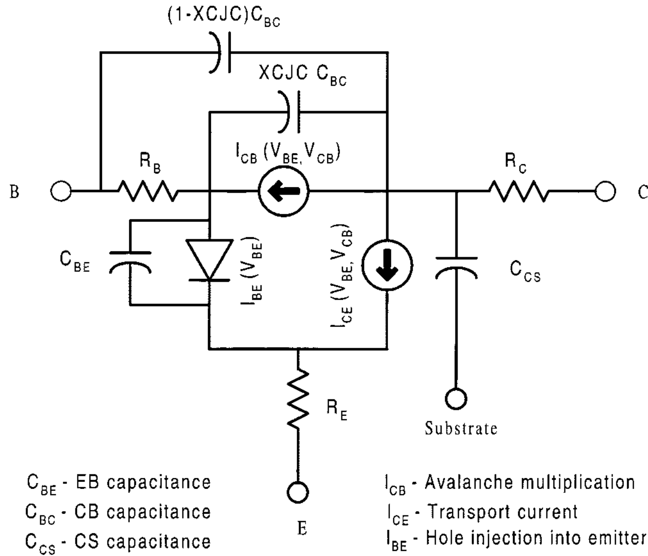

Fig. 1. Equivalent circuit of the SiGe HBT used for Volterra-series simulations.

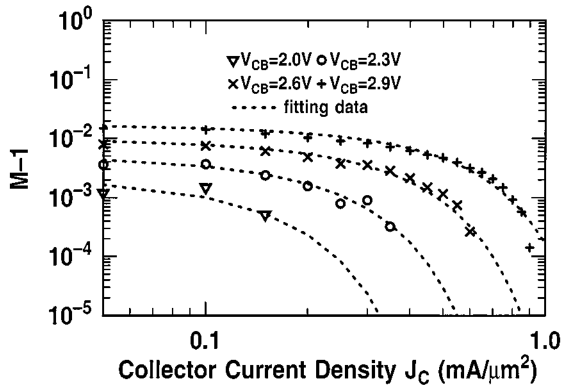

Fig. 2. Comparison of the measured and modeled avalanche multiplication factor $(M-1)$ as a function of J_C for different V_{CB}.

the equivalent-circuit elements were extracted from measured S-parameters, and their derivatives were evaluated numerically. Particular attention was given to the numerical evaluation of the derivatives because of the strong nonlinearity. For instance, the first-order derivative dI_{C0}/dV_{BE} is numerically calculated using $I_{C0}d(\ln I_{C0})/dV_{BE}$, which gives excellent accuracy. The collector-to-substrate junction capacitance in this technology is comparable to the CB junction capacitance and is, therefore, included.

To suppress the Kirk effect, the collector is doped as high as $10^{18}/\mathrm{cm}^3$ in high-speed SiGe HBTs. This results in large avalanche multiplication factor $(M-1)$ and low breakdown voltage. $M-1$ is often modeled only as a function of V_{CB}. In the SiGe HBTs used, $M-1$ is also a strong function of the collector current density J_C, as shown by the measured data in Fig. 2, together with model fitting. We first attempted to apply the $M-1$ model proposed in [11], but could not get satisfactory fitting to the measured $M-1$ for the SiGe HBTs under investigation. The collector doping level in the SiGe HBTs used is

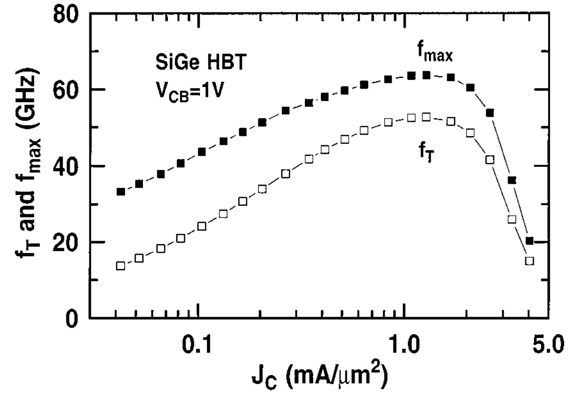

Fig. 3. Measured f_T and $f_{\max}$ as a function of J_C for the SiGe HBTs used in this study.

much higher than in the devices used in [11]. To accurately describe $M-1$ as a function of V_{CB} and J_C in these SiGe HBTs, a new equation was developed as follows:

$$M-1 = \frac{V_{CB}}{\alpha V_{CBO}} \exp\left(-\frac{m\alpha^{-1/3}}{V_{CB}^{2/3}}\right) \quad (2)$$

$$\alpha = 1 - \tanh\left[\frac{I_C}{I_{CO}} \exp\left(\frac{V_{CB}}{V_R}\right)\right] \quad (3)$$

where m, V_{CBO}, I_{CO}, and V_R are fitting parameters.

As shown in Fig. 2, the measured $M-1$ data can be well fitted as a function of collector current density J_C using the proposed $M-1$ equation. As J_C increases, the mobile carrier charge $(-J_C/v)$ compensates the depletion charge (qN_D), which effectively reduces the net charge density on the collector side of the CB junction. The peak electric field in the CB junction thus decreases, resulting in the decrease of $M-1$ with increasing J_C. As expected, the decrease of $M-1$ with J_C varies with V_{CB}.

Another high-injection related effect is the cutoff frequency (f_T) rolloff at high J_C. At sufficiently high J_C, the net charge density reduces to zero, and base push out occurs, resulting in the rolloff of f_T. In SiGe HBTs, the situation is further worsened by the retrograding of an SiGe profile into the collector [12], [13] . Unlike $M-1$, which is strongly dependent on V_{CB}, f_T and $f_{\max}$ are weakly dependent on V_{CB} for $V_{CB} > 0$. Fig. 3 shows the f_T and $f_{\max}$ as a function of J_C measured at $V_{CB} = 1$ V for the same device used in Fig. 2. The f_T and $f_{\max}$ peaks occur near a J_C of 1.0–2.0 mA/μm^2 (Fig. 3), while $M-1$ starts to decrease at much smaller J_C values (see Fig. 2). When base push out occurs (responsible for the f_T and $f_{\max}$ rolloff), the electric field becomes nearly constant in the collector, resulting in a low peak electric field and, hence, a low $M-1$. Past the f_T peak, the electrical CB junction and, hence, the peak electric-field position, shifts from the metallurgical CB junction to the n−epi/n+ buried layer interface. Thus, the peak electric field and $M-1$ increase with J_C past the f_T peak. This increase of $M-1$ with J_C is not included in our new $M-1$ model. In the following, the biasing current is limited to below where f_T peaks, which is the case in many RF circuits.

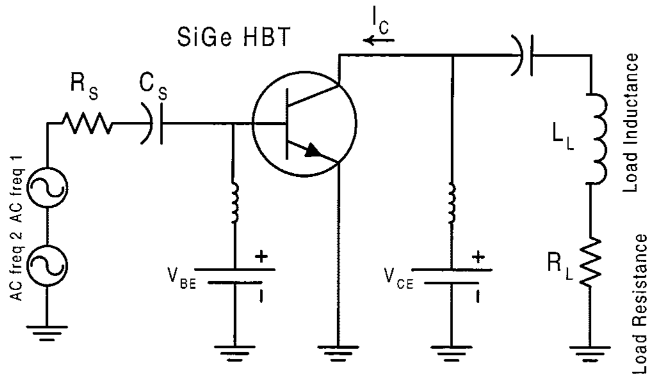

Fig. 4. Circuit schematic of the single transistor amplifier used.

III. Circuit Analysis

A single transistor amplifier shown in Fig. 4 was used for two-tone intermodulation analysis. The SiGe HBT was biased through RF chokes at both the input and output. Capacitors were used to buffer the transistor from the ac source and load. An *RC* series was used for the source, and an *RL* series was used for the load. The large-signal equivalent circuit in Fig. 1 was first linearized at the operating bias. The resulting linear circuit was then solved using compacted modified nodal analysis (CMNA) [14]

$$Y(s) \cdot \vec{H}_1(s) = \vec{I}_1 \tag{4}$$

where $Y(s)$ is the CMNA [14] admittance matrix at frequency $s(j\omega)$, $\vec{H}_1(s)$ is the vector of first-order Volterra kernel transforms of the node voltages, and $\vec{I}_1$ is the vector of the node excitations. The admittance matrix Y and the excitation vector $\vec{I}_1$ were obtained by applying the Kirchoff's current law at every circuit node. The unknowns are the node voltages. The unknown currents associated with zero impedance elements, such as voltage sources, were eliminated in advance [14]. The circuit output and the voltages that control nonlinearities can be expressed as a linear combination of the elements of $\vec{H}_1(s)$.

With $\vec{H}_1(s)$ solved, the same circuit was excited by the second-order nonlinear current sources $\vec{I}_2$, which were determined by the first-order voltages that control individual nonlinearities, and the second-order derivatives of all the I–V and C–V nonlinearities. Every nonlinearity in the original circuit corresponds to a nonlinear current source in parallel with the corresponding linearized circuit element. The orientation of these current sources is the same as the orientation of the controlled current in the original nonlinear circuit. The node voltages under such an excitation are the second-order Volterra kernels $\vec{H}_2(s_1, s_2)$

$$Y(s_1 + s_2) \cdot \vec{H}_2(s_1, s_2) = \vec{I}_2 \tag{5}$$

where $Y(s_1 + s_2)$ is the same CMNA admittance matrix used in (4), but evaluated at the frequency $s_1 + s_2$.

In a similar manner, the third-order Volterra kernels $\vec{H}_3$ were solved as response to excitations specified in terms of the previously determined first- and second-order kernels

$$Y(s_1 + s_2 + s_3) \cdot \vec{H}_2(s_1, s_2, s_3) = \vec{I}_3 \tag{6}$$

P_{out} versus P_{in}, the third-order input intercept (IIP3) at which the first- and third-order signals have equal power, and the (power) gain can then be obtained from $\vec{H}_3$ and $\vec{H}_1$.

In the bipolar transistor model used, $I_{BE}(V_{BE}), C_{BE}(V_{BE})$, $C_{BC}(V_{BE})$, and $C_{CS}(V_{CS})$ depend on only one variable, and have one-dimensional nonlinearity. $I_{CE}(V_{BE}, V_{CB})$ and $I_{CB}(V_{BE}, V_{CB})$ depend on two variables, and have two-dimensional nonlinearity. In total, there are six different kinds of nonlinearity current source excitations. The expressions of the I–V and C–V nonlinearity current sources in terms of the nonlinearity coefficients and nonlinearity control voltages for each order can be found in [3] and [4], where the application of Volterra series to network formulation of nonlinear transfer functions was developed in detail.

In the presence of a multitone input, the node voltages at each mixed frequency for each node can be expressed using the solved Volterra kernels. For a two-tone input $A(\cos\omega_1 t + \cos\omega_2 t)$, the third-order intermodulation (IM3) product at $2\omega_1 - \omega_2$ is given by

$$V_{\text{IM3}} = \frac{3}{4}A^3 H_3(j\omega_1, j\omega_1, -j\omega_2) \tag{7}$$

where H_3 is the third-order Volterra kernel transform of the voltage at the load resistance node (the output node element of $\vec{H}_3$). Similarly, the IM3 product at frequency $2\omega_2 - \omega_1$ can be calculated. The frequency difference between $2\omega_1 - \omega_2$ and $2\omega_2 - \omega_1$ is typically so small that the corresponding IM3 have equal magnitude.

The output voltage at the fundamental frequency ω_1 is given by

$$V_{\text{fundamental}} = AH_1(j\omega_1) \tag{8}$$

where $H_1(j\omega_1)$ is the output node element of $\vec{H}_1(j\omega_1)$. $H_1(j\omega_1)$ is essentially the voltage gain, from which the power gain can be calculated together with the source and load impedance values. The input voltage magnitude A_{IP3}, at which the extrapolated fundamental output voltage equals the intermodulation output voltage, is obtained by equating (7) and (8) as follows:

$$A_{\text{IP3}} = \sqrt{\frac{4}{3} \cdot \frac{|H_3(j\omega_1, j\omega_1, -j\omega_2)|}{|H_1(j\omega_1)|}} \tag{9}$$

Accordingly, IIP3, the input power at which the fundamental output power equals the intermodulation output power, is obtained as

$$\text{IIP3} = \frac{A_{\text{IP3}}^2}{8R_S} = \frac{1}{6R_S} \cdot \frac{|H_3(j\omega_1, j\omega_1, -j\omega_2)|}{|H_1(j\omega_1)|} \tag{10}$$

where R_S is the source resistance. IIP3 is often expressed in dBm by $\text{IIP3}_{\text{dBm}} = 10\log_{10}\left(10^3 \cdot \text{IIP3}\right)$.

IV. Identifying Dominant Nonlinearity

One of the major advantage of the Volterra-series approach is the ability to identify the dominant nonlinearity [4]. The identification is traditionally realized by separating $\vec{H}_3$ into several components related to each individual nonlinearity [4]. The

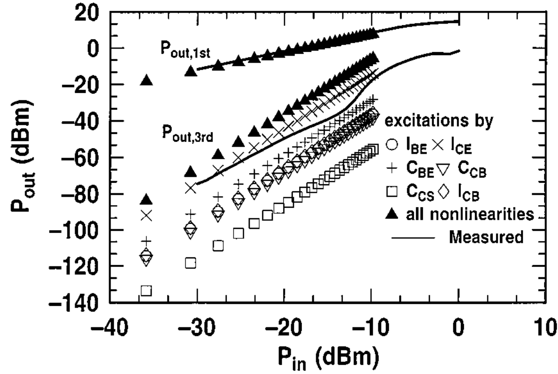

Fig. 5. Comparison of the simulated and measured $P_{\rm out}$ versus $P_{\rm in}$ at 2 GHz for a single-transistor SiGe HBT amplifier. $A_E = 0.5 \times 20 \times 4\ \mu\text{m}^2$. $I_C = 3$ mA, $V_{CE} = 3$ V, $R_S = 50\ \Omega$, $C_S = 300$ pF, $R_L = 186\ \Omega$, $L_L = 9$ nH. Tone spacing is 1 MHz.

overall $\vec{H}_3$ is simply the sum of the individual $\vec{H}_3$. This, however, does not completely distinguish individual nonlinearities because the solution of $\vec{H}_2$ involves all the nonlinearities, and $\vec{H}_2$ was used in the calculation of $\vec{I}_3$.

To completely distinguish individual nonlinearities, here we propose a new approach. For each nonlinearity, both $\vec{H}_2$ and $\vec{H}_3$ are solved using *only* the virtual current source excitation related to the specific nonlinearity in question. Thus, an individual IIP3 is obtained for each nonlinearity. The individual nonlinearity that gives the lowest IIP3 (the worst linearity) is identified as the dominant nonlinearity.

We then calculate the overall IIP3 by including all of the nonlinearities in the calculation of both $\vec{H}_2$ and $\vec{H}_3$. A comparison of the individual IIP3 and the overall IIP3 reveals the interaction between individual nonlinearities. As shown later, the overall IIP3 obtained by including all of the nonlinearities can be larger (better) than an individual IIP3, implying cancellation between individual nonlinearities. Unlike as in the traditional approach, the overall $\vec{H}_3$ is not equal to the sum of all of the individual $\vec{H}_3$ because of the complete separation of individual nonlinearities.

V. Results and Discussion

A. Comparison With Measurement

Volterra series is only applicable to low input power, such as the signal levels found at a mobile receiver (as low as -100 dBm). IIP3 measurements, however, are often made at much higher $P_{\rm in}$ to improve measurement accuracy. Volterra series is less accurate for these measurement conditions. Nevertheless, a comparison with measurement still provides a test of the accuracy of the simulation, and is shown in Fig. 5. The frequency is 2 GHz, and the tone spacing is 1 MHz. The SiGe HBT has four $A_E = 0.5 \times 20\ \mu\text{m}^2$ emitter fingers, i.e., $I_C = 3$ mA, $V_{CE} = 3$ V, $R_S = 50\ \Omega$, $C_S = 300$ pF, $R_L = 186\ \Omega$, and $L_L = 9$ nH. The agreement with measurement is excellent for the fundamental signal, and is within 5 dB for the intermodulation signal at $P_{\rm in} = -30$ dBm. This is acceptable considering that -30 dBm is "large" for the small-signal distortion requirement.

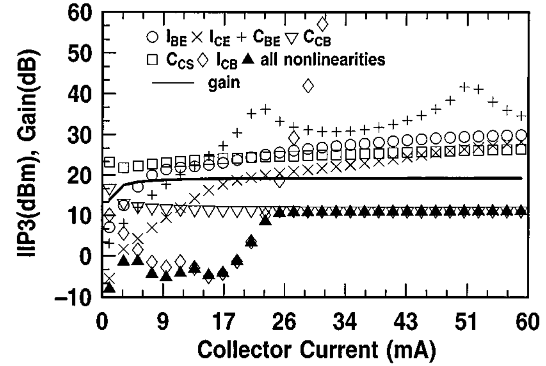

Fig. 6. IIP3 and gain as a function of I_C.

B. Collector Current Dependence

Fig. 6 shows the IIP3 and gain as a function of I_C up to 60 mA at which f_T and $f_{\max}$ peak. The collector biasing voltage is $V_{CE} = 3$ V. At low I_C (< 5 mA), the exponential $I_{CE} - V_{BE}$ nonlinearity ($\times$) yields the lowest individual IIP3 and, hence, is the dominant factor. For 5 mA $< I_C <$ 25 mA, the I_{CB} nonlinearity due to avalanche multiplication ($\diamond$) dominates. For $I_C > 25$ mA, the C_{CB} nonlinearity due to the CB capacitance ($\bigtriangledown$) dominates. Interestingly, the overall IIP3 obtained by including all of the nonlinearities is close to the lowest individual IIP3 for all the I_C in this case. The closeness indicates a weak interaction between individual nonlinearities.

The overall IIP3 increases with I_C for $I_C < 5$ mA when the exponential I_{CE} nonlinearity dominates. For $I_C > 5$ mA where the avalanche current (I_{CB}) nonlinearity dominates, the I_C dependence of the overall IIP3 is twofold as follows.

- The initial current for avalanche I_{CE} increases with I_C.
- The avalanche multiplication factor $(M - 1)$ decreases with I_C.

Even though the details of the simulated overall IIP3 curve cannot be easily explained, the increase of the avalanche IIP3 and, hence, the overall IIP3 for $I_C > 17$ mA can be readily understood as a result of the decrease of $M - 1$ with increasing J_C. For $I_C > 25$ mA, **the overall IIP3 becomes limited by the C_{CB} nonlinearity, and is approximately independent of I_C.** The optimum biasing current is, therefore, $I_C = 25$ mA in this case ($V_{CE} = 3$ V). The use of a higher I_C only increases power consumption, and does not improve linearity. The decrease of $M - 1$ with increasing J_C is, therefore, beneficial to the linearity of these SiGe HBTs. To our knowledge, this is the only beneficial effect of the charge compensation by mobile carriers in the CB junction space charge region. Our simulation results also indicate the importance of modeling the J_C dependence of $M - 1$ for linearity analysis of SiGe HBT circuits.

To minimize noise, low-noise amplifiers in this technology are typically biased at a J_C of 0.1–0.2 mA/μm^2, which corresponds to a I_C of 4–8 mA in Fig. 6. In this I_C range, IIP3 is limited by avalanche multiplication for the circuit configuration in Fig. 4. For further improvement of the IIP3, a lower collector doping is desired, provided that the noise performance is not inadvertently degraded. Our earlier research showed that the noise figure is relatively independent of the collector doping as long as the Kirk effect does not occur at the J_C of interest [16]. Thus,

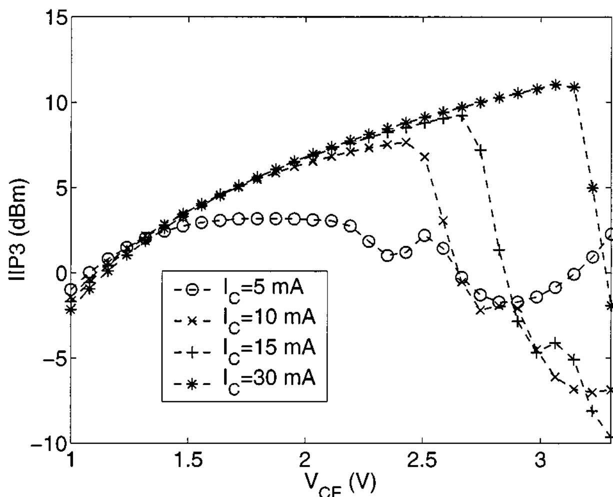

Fig. 7. IIP3 as a function of V_{CE} for different I_C.

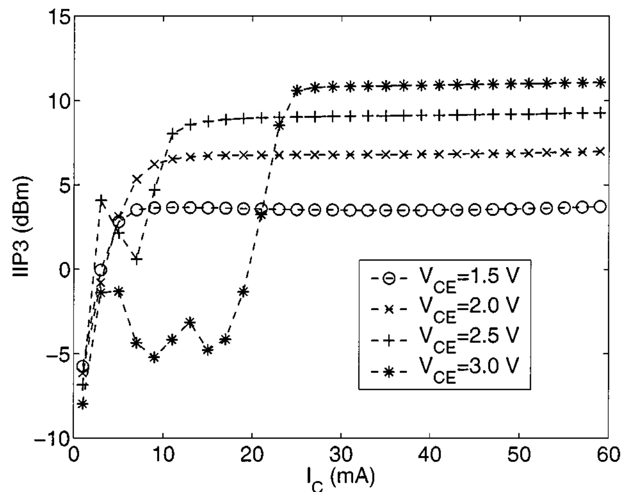

Fig. 8. IIP3 as a function of I_C for different V_{CE}.

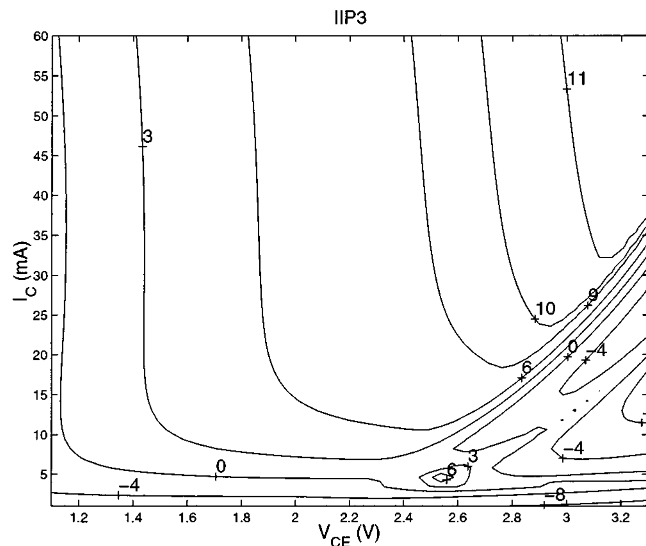

Fig. 9. Contours of the IIP3 in dBm on the I_C–V_{CE}-plane.

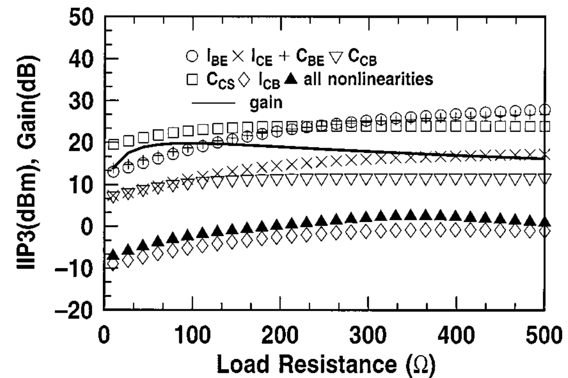

Fig. 10. IIP3 and gain as a function of load resistance at $I_C = 13$ mA and $V_{CE} = 3$ V.

there must exist an optimum collector doping profile for producing low-noise transistors with the best linearity.

C. Collector Voltage Dependence

An alternative to the use of lower collector doping for smaller $M-1$ is to reduce the collector biasing voltage at the expense of a reduced output voltage swing or dynamic range. However, the reduction of collector biasing voltage enhances the CB capacitance nonlinearity as well. Therefore, one must carefully optimize the collector biasing voltage for optimum IIP3. Fig. 7 shows the overall IIP3 as a function of V_{CE} up to 3.3 V, the BV_{CEO} of the transistor. A peak of IIP3 generally exists as V_{CE} increases. For $I_C = 10$ mA where the noise figure is minimum, the optimum biasing V_{CE} is 2.4 V, yielding an IIP3 of 9 dBm. The IIP3 obtained (9 dBm) is 11 dB higher than the IIP3 at $V_{CE} = 3$ V $(-2$ dBm$)$, illustrating the importance of biasing in determining linearity of these SiGe HBTs.

To better illustrate the importance of biasing current and voltage selection, the IIP3 is shown as a function of I_C for different V_{CE} in Fig. 8. As discussed earlier, at sufficiently high I_C, the IIP3 approaches a value that depends on V_{CE}. The threshold I_C where the IIP3 reaches its maximum is higher for a higher V_{CE}. For a given V_{CE}, I_C must be above the threshold to achieve good IIP3. On the other hand, the use of an I_C well above the threshold does not further increase IIP3, and only increases power consumption. Thus, the optimum I_C is at the threshold value, which is 10 mA for $V_{CE} = 2$ V. Fig. 9 shows contours of the IIP3 as a function of I_C and V_{CE}, which can be used for the selection of biasing current and voltage.

D. Load Dependence and Cancellation Between C_{CB} and I_{CB} Nonlinearities

Fig. 10 shows the IIP3 simulated with individual and all nonlinearities versus load resistance. Gain varies with load, and peaks when the load is closest to conjugate matching, as expected. IIP3, however, is much more sensitive to load variation. The IIP3 with all nonlinearities (denoted by ▲) is noticeably higher than the IIP3 with the avalanche current (I_{CB}) nonlinearity alone (denoted by ◇). The interaction between individual nonlinearities has **improved** the overall linearity through cancellation. In this case, the two most dominating nonlinearities are the avalanche current I_{CB} nonlinearity and the C_{CB} nonlinearity. The cancellation between the I_{CB} and C_{CB} nonlinearities leads to an overall IIP3 value that is higher (better) than the IIP3 obtained using the I_{CB} nonlinearity alone. The degree of cancellation depends on

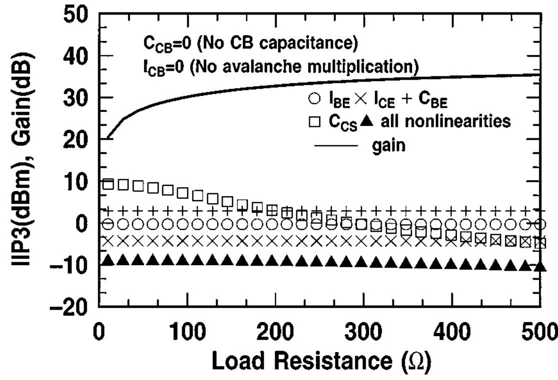

Fig. 11. IIP3 and gain versus load resistance at $I_C = 13$ mA and $V_{CE} = 3$ V. $C_{CB} = 0$ and $I_{CB} = 0$.

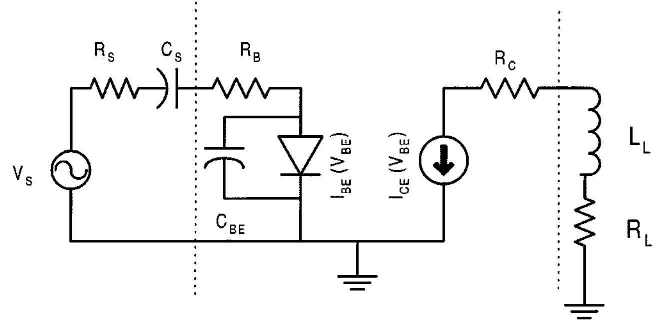

Fig. 12. Equivalent circuit of a single transistor amplifier with $C_{CB} = 0$, $I_{CB} = 0$, and $F_{\mathrm{Early}} = 1$.

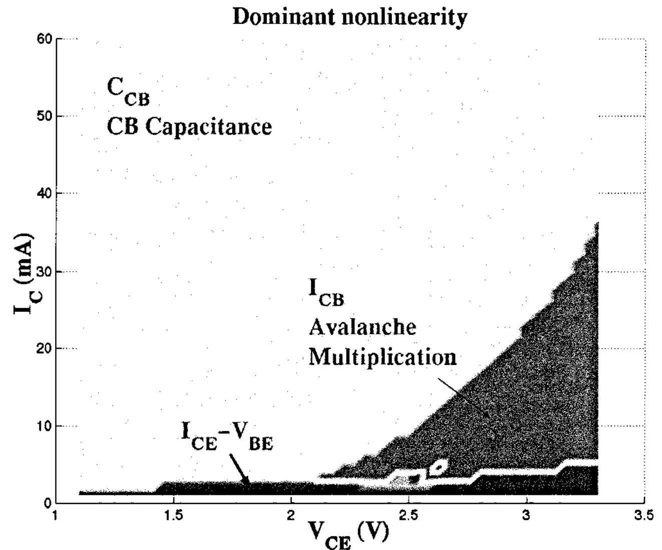

Fig. 13. Dominant nonlinearity factor on the I_C–V_{CE}-plane.

the biasing, source, and load conditions, as expected from the Volterra-series theory. The cancellation between I_{CE} and C_{BE} analyzed in [15] is not important in this case.

Physically, we attribute the load dependence of linearity in these HBTs to the CB feedback. The first kind of such feedback is the CB capacitance C_{CB}, and the second kind is the avalanche multiplication current I_{CB} that flows from the collector to base. Both feedbacks are nonlinear, though the load dependence would still exist for linear CB feedback [17] (for instance, externally connected linear CB capacitance). Another kind of feedback is the emitter resistance. The emitter resistance feedback is negligible in these devices because of low emitter resistance. The Early effect contribution to the load dependence is also small because of the large Early voltage in these HBTs. Another contributor to the load dependence of the transistor linearity is the collector–substrate capacitance (C_{CS}) nonlinearity. The underlying reason is that the nonlinearity controlling voltage V_{CS} is a function of the load condition. The contribution of C_{CS} nonlinearity to the overall IIP3, however, is generally negligible because of its placement in the equivalent circuit.

For verification, the simulation was repeated by setting $C_{CB} = 0$ and $I_{CB} = 0$. The experimentally extracted F_{Early} and R_E were used. The results in Fig. 11 support our speculation. The IIP3 becomes virtually independent of load for all of the nonlinearities, except for the C_{CS} nonlinearity. Closed-form analysis using Volterra series for a transistor with zero C_{CB}, zero I_{CB}, and zero R_e indeed proves that the IIP3 becomes independent of the load conditions when these feedbacks are removed. The mathematical proof is not given here due to space limitations. The underlying physics, however, is straightforward if we examine the corresponding equivalent circuit shown in Fig. 12. An inspection of the nonlinear circuit shows that the voltage V_{BE} that controls the $I_{BE} - V_{BE}$, $C_{BE} - V_{BE}$ and $I_{CE} - V_{BE}$ nonlinearities becomes independent of the load condition when $C_{CB} = 0$, $I_{CB} = 0$, $R_E = 0$. Due to the weak Early effect in HBTs, the nonlinear current I_{CE} is solely determined by V_{BE} and, therefore, also independent of the load condition. As a result, the IIP3 becomes independent of the load condition.

E. Linearity Limiting Factors

Fig. 13 shows the dominant nonlinearity factor on the I_C–V_{CE}-plane. The source and load conditions are the same as in Fig. 5. However, the results obtained using other load conditions are similar. The upper limit of I_C is where f_T reaches its peak value. Avalanche multiplication and C_{CB} nonlinearities are the dominant factors for most of the bias currents and voltages. From device physics, both avalanche multiplication and C_{CB} nonlinearities can be reduced by reducing the collector doping. This conflicts with the need for high collector doping to suppress the Kirk effect and heterojunction barrier effects in SiGe HBTs. Therefore, multiple collector doping profiles are needed to provide both high f_T devices and high IIP3 devices for different stages of the same circuit. In processing, this can be achieved by selective ion implantation in forming the collector.

VI. Summary

A systematic analysis of the RF intermodulation in SiGe HBTs is performed using a new Volterra series-based approach. The relative dominance of individual nonlinearities and their interaction were shown to vary with load, biasing current and voltage, and CB feedback. The C_{CB} and avalanche multiplication feedbacks are responsible for the load dependence. A cancellation mechanism between the avalanche current (I_{CB}) nonlinearity and the CB capacitance (C_{CB}) nonlinearity is identified. The avalanche multiplication nonlinearity dominates at low I_C, and the CB capacitance nonlinearity dominates at

high I_C. The decrease of the avalanche multiplication factor $(M-1)$ with increasing I_C is significant in determining the linearity of these SiGe HBTs, and must be modeled for circuit simulation. Guidelines are obtained for selecting the biasing current and voltage (I_C and V_{CE}) that are optimum for maximum IIP3 with low power consumption. The results suggest that there is a fundamental limit to achieving high f_T and high linearity, and multiple collector profiles are desired for leverage in RF circuit design.

ACKNOWLEDGMENT

The authors would like to thank D. Ahlgren, S. Subbanna, N. King, W. Ansley, and B. Meyerson, all of IBM Microelectronics, East Fishkill, NY, A. J. Joseph, IBM Microelectronics, Essex Junction, VT, and S. Taylor, Maxim, Hillsboro, OR, for their contributions. The wafers were fabricated at IBM Microelectronics, Essex Junction, VT.

REFERENCES

[1] K. Kundert, J. White, and A. Sangiovanni-Vincentelli, *Steady-State Methods for Simulating Analog and Microwave Circuits*. Norwell, MA: Kluwer, 1990.

[2] V. Volterra, *Theory of Functionals and of Integral and Integro-Differential Equations*. New York: Dover, 1959.

[3] D. D. Weiner and J. E. Spina, *Sinusoidal Analysis and Modeling of Weakly Nonlinear Circuits*. New York: Van Nostrand, 1980.

[4] P. Wambacq and W. Sansen, *Distortion Analysis of Analog Integrated Circuits*. Norwell, MA: Kluwer, 1998.

[5] S. Narayanan, "Transistor distortion analysis using Volterra series representation," *Bell Syst. Tech. J.*, vol. 46, no. 3, pp. 991–1024, May–June 1967.

[6] ——, "Application of Volterra series to intermodulation distortion analysis of transistor feedback amplifiers," *IEEE Trans. Circuit Theory*, vol. CT-17, pp. 518–527, Nov. 1970.

[7] S. Narayanan and H. C. Poon, "An analysis of distortion in bipolar transistors using integral charge-control model and Volterra series," *IEEE Trans. Circuit Theory*, vol. CT-20, pp. 341–351, July 1973.

[8] H. C. Poon, "Modeling of bipolar transistor using integral charge-control model with application to third-order distortion studies," *IEEE Trans. Electron Devices*, vol. ED-19, pp. 719–731, June 1972.

[9] D. C. Ahlgren, M. Gilbert, D. Greenberg, S. J. Jeng, J. Malinowski, D. Nguyen-Ngoc, K. Schonenberg, K. Stein, R. Groves, K. Walter, G. Hueckel, D. Colavito, G. Freeman, D. Sunderland, D. L. Harame, and B. Meyerson, "Manufacturability demonstration of an integrated SiGe HBT technology for the analog and wireless marketplace," in *Tech. Dig. IEDM*, 1996, pp. 859–862.

[10] G. F. Niu, J. D. Cressler, S. Zhang, U. Gogineni, and D. C. Ahlgren, "Measurement of collector–base junction avalanche multiplication effect in advanced UHV/CVD SiGe HBT's," *IEEE Trans. Electron Devices*, vol. 46, pp. 1007–1015, May 1999.

[11] W. J. Kloosterman, J. C. J. Paasschens, and R. J. Havens, "A comprehensive bipolar avalanche multiplication compact model for circuit simulation," in *Proc. IEEE BCTM*, 2000, pp. 172–175.

[12] A. J. Joseph, J. D. Cressler, D. M. Richey, and G. F. Niu, "Optimization of SiGe HBT's for operation at high current densities," *IEEE Trans. Electron Devices*, vol. 46, pp. 1347–1354, July 1999.

[13] G. F. Niu and J. D. Cressler, "The impact of bandgap offset distribution between conduction and valence bands in Si-based graded bandgap HBT's," *Solid State Electron.*, vol. 43, no. 12, pp. 2225–2230, Dec. 1999.

[14] G. Gielen and W. Sansen, *Symbolic Analysis for Automated Design of Analog Integrated Circuits*. Norwell, MA: Kluwer, 1991.

[15] S. Maas, B. Nelson, and D. Tait, "Intermodulation in heterojunction bipolar transistors," *IEEE Trans. Microwave Theory Tech.*, vol. 40, pp. 442–448, Mar. 1992.

[16] G. F. Niu, W. E. Ansley, S. Zhang, J. D. Cressler, C. Webster, and R. Groves, "Noise parameter optimization of UHV/CVD SiGe HBT's for RF and microwave applications," *IEEE Trans. Electron Devices*, vol. 46, pp. 1347–1354, Aug. 1999.

[17] G. F. Niu, J. D. Cressler, W. E. Ansley, C. S. Webster, R. Anna, and N. King, "Intermodulation characteristics of UHV/CVD SiGe HBT's," in *Proc. IEEE BCTM*, Sept. 1999, pp. 50–53.

Guofu Niu (M'98) was born in Henan, China, in December 1971. He received the B.S. (with honors), M.S., and Ph.D. degrees in electrical engineering from Fudan University, Shanghai, China, in 1992, 1994, and 1997, respectively.

From December 1995 to January 1997, he was a Research Assistant at the City University of Hong Kong, where he worked on mixed-level device/circuit simulation and quantum-effect programmable logic gates. From May 1997 to May 2000, he conducted post-doctoral research at Auburn University, Auburn, AL, where he focused on SiGe RF devices. In June 2000, he joined the faculty of Auburn University, where he is currently an Associate Professor of Electrical and Computer Engineering. His research interests include SiGe devices and circuits, noise, radiation effects, SiC devices, low-temperature electronics, and technology computer-aided design (TCAD). He has authored or co–authored over 30 journal papers and over 30 conference papers related to his research. He is listed in *Who's Who in America.*

Dr. Niu served on the Program Committee of the 1997 Asia–South-Pacific Design Automation Conference (ASP-DAC). He has served as a technical reviewer for the IEEE ELECTRON DEVICE LETTERS, the IEEE TRANSACTIONS ON ELECTRON DEVICES, the IEEE JOURNAL OF SOLID-STATE CIRCUITS, and the IEEE MICROWAVE AND GUIDED WAVE LETTERS.

Qingqing Liang was born in Hunan, China, on September 20, 1977. He received the B.S. and M.S. degrees in electrical engineering from Fudan University, Shanghai, China, in 1997 and 2000, respectively, and is currently working toward the Ph.D. degree in electrical and computer engineering at Auburn University, Auburn, AL.

His research focuses on the optimization of SiGe HBT devices and circuit building blocks for RF and microwave applications.

John D. Cressler (S'86–A'91–SM'91–F'01) received the B.S. degree in physics from the Georgia Institute of Technology, Atlanta, in 1984, and the M.S. and Ph.D. degrees in applied physics from Columbia University, New York, NY, in 1987 and 1990, respectively.

From 1984 to 1992, he was on the research staff at the IBM Thomas J. Watson Research Center, Yorktown Heights, NY, where he was involved with high-speed Si and SiGe bipolar technology. In 1992, he joined the faculty of Auburn University, Auburn, AL, where he is currently a Philpott–Westpoint Stevens Distinguished Professor of Electrical and Computer Engineering and Director of the Alabama Microelectronics Science and Technology Center, a multidisciplinary state-funded research center. His research interests include SiGe HBT and FET device physics, radiation effects, noise, linearity, cryogenic electronics, SiC devices and technology, Si-based RF/microwave circuits, reliability physics, device simulation, and compact circuit modeling. He has authored or co-authored over 220 technical papers related to his research and has written four book chapters. He holds one patent. He has served as a Consultant to IBM, Analog Devices, Northop-Grumman, ITRI/ERSO,Taiwan, R.O.C., Teltech, the National Technological University, Commercial Data Servers, MEMS-Optical, ON Semiconductor, and Texas Instruments Incorporated.

Dr. Cressler is an associate editor for the IEEE JOURNAL OF SOLID-STATE CIRCUITS. He served on the Technical Program Committees of the International Solid-State Circuits Conference (ISSCC) (1992–1998, 1999-present), the Bipolar/BiCMOS Circuits and Technology Meeting (BCTM) (1995–1999), the International Electron Devices Meeting (IEDM) (1996–1997), and the Nuclear and Space Radiation Effects Conference (NSREC) (1999–2000). He was the Technical Program chairman of the 1998 ISSCC. He is currently chair of the Technology Directions Subcommittee, ISSCC, and is on the Executive Steering Committee for the IEEE Microwave Theory and Techniques Society (IEEE MTT-S) Topical Meeting on Silicon Monolithic Integrated Circuits in RF Systems. He is an IEEE Electron Device Society Distinguished Lecturer. He was the recipient of the 1996 C. Holmes MacDonald National Outstanding Teacher Award presented by Eta Kappa Nu, the 1996 Auburn University Alumni Engineering Council Research Award, the 1998 Auburn University Birdsong Merit Teaching Award, the 1999 Auburn University Alumni Undergraduate Teaching Excellence Award, the IEEE Millennium Medal in 2000, and the 1994 Office of Naval Research Young Investigator Award for his SiGe research program. He was also the recipient of five awards presented by the IBM Research Division.

Charles S. Webster (M'89) received the B.A. and M.S. degrees in physics from the University of Vermont, Burlington, in 1981 and 1985, respectively, and the M.S. degree in nuclear engineering sciences concentrating in radiological physics from the University of Florida, Gainsville, in 1995.

He is currently with the RF/Analog Development Group, IBM Microelectronics, Essex Junction, VT, where he specializes in RF and microwave characterization techniques.

David L. Harame (S'77–M'83) was born in Pocatello, ID, in 1948. He received the B.A. degree in zoology from the University of California at Berkeley, in 1971, the M.S. degree in zoology from Duke University, Durham, NC, in 1973, the M.S. degree in electrical engineering from San Jose State University, San Jose, CA, in 1976, and the M.S. degree in materials science and the Ph.D. degree in electrical engineering from Stanford University, Stanford, CA, in 1984.

In 1984, he joined the Bipolar Technology Group, IBM T. J. Watson Research Center, Yorktown Heights, NY, where he was involved with the fabrication and modeling of silicon-based integrated circuits. His specific research interests at the T. J. Watson Research Center included silicon and SiGe-channel FET transistors, n-p-n and p-n-p SiGe-based bipolar transistors, complementary bipolar technology, and BiCMOS technology for digital, analog, and mixed-signal applications. In 1993, he joined the Semiconductor Research and Development Center, Advanced Semiconductor Technology Center (ASTC), IBM, Hopewell Junction, NY, where he was responsible for the development of SiGe technology for mixed-signal applications. He managed SiGe BiCMOS technology development at the ASTC through 1997. In 1998, he joined the IBM Manufacturing Organization, Essex Junction, VT, where he managed an SiGe technology group and installed the SiGe BiCMOS process in the manufacturing line. In 1999, he rejoined the Semiconductor Research Center, while remaining in Essex Junction, VT. He is currently a Senior Technical Staff Member of IBM, and manages an SiGe BiCMOS development group.

Dr. Harame is a member of the Bipolar/BiCMOS Circuits and Technology Meeting Executive Committee.